Hydrogen-related excitons and their excited-state transitions in ZnO

R. Heinhold,[1,2] A. Neiman,[2,3] J. V. Kennedy,[2,4] A. Markwitz,[2,4] R. J. Reeves,[2,3] and M. W. Allen[1,2,*]

[1]*Department of Electrical and Computer Engineering, University of Canterbury, Christchurch 8014, New Zealand*

[2]*The MacDiarmid Institute for Advanced Materials and Nanotechnology, New Zealand*

[3]*Department of Physics and Astronomy, University of Canterbury, Christchurch 8014, New Zealand*

[4]*National Isotope Centre, GNS Science, P.O. Box 31312, Lower Hutt 5010, New Zealand*

(Received 21 November 2016; revised manuscript received 10 January 2017; published 23 February 2017)

The role of hydrogen in the photoluminescence (PL) of ZnO was investigated using four different types of bulk ZnO single crystal, with varying concentrations of unintentional hydrogen donor and Group I acceptor impurities. Photoluminescence spectra were measured at 3 K, with emission energies determined to $\pm 50\ \mu$eV, before and after separate annealing in O_2, N_2, and H_2 atmospheres. Using this approach, several new hydrogen-related neutral-donor-bound excitons, and their corresponding *B* exciton, ionized donor, and two electron satellite (TES) excited state transitions were identified and their properties further investigated using hydrogen and deuterium ion implantation. The commonly observed I_4 (3.36272 eV) emission due to excitons bound to multicoordinated hydrogen inside an oxygen vacancy (H_O), that is present in most ZnO material, was noticeably absent in hydrothermally grown (HT) ZnO and instead was replaced by a doublet of two closely lying recombination lines $I_{4b,c}$ (3.36219, 3.36237 eV) due to a hydrogen-related donor with a binding energy (E_D) of 47.7 meV. A new and usually dominant recombination line $I_{6\text{-}H}$ (3.36085 eV) due to a different hydrogen-related defect complex with an E_D of 49.5 meV was also identified in HT ZnO. Here, $I_{4b,c}$ and $I_{6\text{-}H}$ were stable up to approximately 400 and 600 °C, respectively, indicating that they are likely to contribute to the unintentional *n*-type conductivity of ZnO. Another doublet I_5 (3.36137, 3.36148 eV) was identified in hydrogenated HT ZnO single crystals with low Li concentrations, and this was associated with a defect complex with an E_D of 49.1 meV. A broad near band edge (NBE) emission centered at 3.366 eV was associated with excitons bound to subsurface hydrogen. We further demonstrate that hydrogen incorporates on different lattice sites for different annealing conditions and show that the new features $I_{4b,c}$, $I_{6\text{-}H}$, and I_5 most likely originate from the lithium-hydrogen defect complexes Li_{Zn}-H_O, Al_{Zn}-H_O-Li_{Zn}, and V_{Zn}-$H_{3,4}$, respectively.

DOI: 10.1103/PhysRevB.95.054120

I. INTRODUCTION

Hydrogen is a ubiquitous defect found in nearly all semiconductors [1–3]. It is highly mobile and is unavoidably introduced during material growth and processing as it is usually a significant residual contaminant in most vacuum deposition systems [4,5]. In most materials, hydrogen is amphoteric in nature, tending to counteract the prevailing conductivity caused by other impurities and defects [5,6]. This behavior was explained by Van de Walle and Neugebauer [6], by considering the Fermi-level position $\varepsilon(+/-)$ at which the donor (H^+) and acceptor (H^-) forms of hydrogen have the same formation energies. In most semiconductors, the $\varepsilon(+/-)$ level lies within the band gap, and consequently, the formation of H^+ is energetically favored in *p*-type material and H^- in *n*-type material [6]. The same authors also showed that, in the case of ZnO, the $\varepsilon(+/-)$ level lies above the conduction band minimum, and in this case, only H^+ is stable, and hydrogen behaves exclusively as a donor, capable of providing a significant contribution to the unintentional *n*-type conductivity of ZnO [6,7].

Hydrogen's role as a shallow donor in ZnO was first recognized in the 1950s when the hydrogenation of ZnO was shown to increase its *n*-type conductivity [8,9]. Since then, many different hydrogen donors have been identified in ZnO, primarily by infrared (IR) and Raman spectroscopy, with considerable debate concerning their relative contribution to its unintentional *n*-type conductivity. Theoretical support for the behavior of hydrogen as a shallow donor in ZnO was provided by the first-principles density functional theory (DFT) calculations of Van de Walle [7], who showed that both interstitial hydrogen (H_i) and substitutional H located on the oxygen lattice site (H_O) were shallow donors. Janotti and Van de Walle [10] subsequently showed that H_O involves multicentered bonding between an H atom and all four Zn nearest neighbor atoms and proposed that tetrahedrally coordinated H_O plays a significant role in the unintentional *n*-type conductivity of ZnO, explaining the latter's thermal stability and oxygen partial pressure dependence. Further support for this argument was provided by the first-principles calculations of Wardle *et al.* [11] that predicted H_i to be mobile at low temperatures in ZnO and that thermally stable hydrogen donors must therefore be associated with hydrogen trapped at secondary defects. Lavrov *et al.* [12] experimentally identified two shallow hydrogen donors in hydrogenated vapor-phase (VP) grown ZnO single crystals using a combination of Raman, IR, photoluminescence (PL), and photoconductivity spectroscopy: These were interstitial bond-centered hydrogen (H_{BC}) with an ionization energy of 53 meV and H_O with an ionization energy of 47 meV [12]. The same authors also showed that H_{BC} is unstable against thermal treatment at 190 °C and forms a reservoir of electrically inactive hidden H_2 molecules [13] that, as initially proposed by Shi *et al.* [14], can be incorporated into other defect complexes during subsequent thermal treatment. In contrast, H_O has a significantly higher

*Corresponding author: martin.allen@canterbury.ac.nz

 ©2017 American Physical Society

TABLE I. Hydrogen-related defects identified via (a) IR and Raman spectroscopy, and (b) PL spectroscopy, with their physical assignment and upper thermal stability limit (temp. limit).

	Assignment	Temp. limit (°C)	Ref.
(a) IR/Raman line (cm^{-1})			
742/792	H_O	500–700	[12,15,16]
3326/3358	XH	—	[17–19]
3577.3	Li-H-O	1200	[20–23]
3611	H_{BC}	150–190	[12]
4145	H_2	300–700	[13,24]
3312/3349	V_{Zn}-H_2	—	[25]
3303/3321	V_{Zn}-H_3	750	[26]
(b) PL Line (eV)			
3.3628 (I_4)	H_O	500–700	[12]
3.3601	H_{BC}	150–190	[12]
3.3610/3.3617	V_{Zn}-$H_{3,4}$	—	[27–29]

thermal stability (typically up to 600 °C) than H_{BC} as its multicentered bonding makes it more stable against thermal dissociation [15,16]. Other H-related defect complexes identified via IR and Raman spectroscopy include single and multihydrogenated zinc vacancies (V_{Zn}-H_n), hydrogen-lithium complexes (Li-H-O), and an unknown defect XH involving OH bonds. A complete list of hydrogen-related defects identified via Raman and IR spectroscopy is given in Table I.

Hydrogen is also present at the surface of ZnO in the form of an ubiquitous hydroxyl termination of the bulk lattice that causes the conduction and valence bands to bend downwards, thereby creating a potential well in which a two-dimensional surface electron accumulation layer is confined [30–32]. We have recently shown a direct association between the extent of the hydroxyl termination and the downward band bending of the surface electronic bands [31,32], while Piper *et al.* [33] and Ozawa and Mase [34] have found evidence of quantized states inside the hydroxyl-induced potential wells at ZnO surfaces.

Although many different forms of hydrogen have been identified in ZnO via IR and Raman spectroscopy (Table I), far less is known about the role of hydrogen in the PL of ZnO, despite the fact that it is an intense ultraviolet (UV) emitter. Photoluminescence is a sensitive probe of the discrete electronic states introduced by impurities and defects. Furthermore, the large binding energy (60 meV) and lifetime of free excitons in ZnO allows them to bind to a wide range of lattice defects, resulting in a highly rich PL spectra [35–37]. Despite this, only a few hydrogen-related excitonic features have been identified in ZnO, and these are also given in Table I: The most commonly observed feature is the I_4 line (3.3628 eV) that was first associated with hydrogen by Meyer *et al.* [36] and subsequently assigned to the recombination of an exciton bound to the H_O shallow donor defect [12]. Other reported hydrogen-related features, include a recombination line at 3.3601 eV due to an exciton bound to H_{BC} [12] and recombination lines at 3.3617 and 3.3610 eV that were associated with defects involving multiple O-H bonds inside a Zn vacancy (V_{Zn}-H_n) [27–29].

In this paper, we present a detailed investigation of the role of hydrogen in the PL of ZnO via a comparative study of four different types of bulk single crystal with different hydrogen and lithium impurity concentrations. Freestanding ZnO single crystals were used as their high crystallinity, low defect density, and the lack of substrate-induced strain results in very narrow line-width radiative transitions, allowing the perturbations caused by the incorporation of hydrogen in defect complexes to be resolved. These crystals were selectively annealed in N_2, O_2, and forming gas (FG; both N_2/H_2 and Ar/H_2) and implanted with hydrogen and deuterium. Several new hydrogen-related neutral donor-bound excitons, $I_{6\text{-}H}$ (3.36085 eV), I_5 (3.36137, 3.36148 eV), $I_{4b,c}$ (3.36219, 3.36237 eV), and their excited state transitions were identified, along with their associated donor binding energies and thermal stability.

II. EXPERIMENTAL

A. Bulk ZnO single crystals

ZnO single crystal wafers (dimension $10 \times 10 \times 0.5\ mm^3$) grown via three different bulk crystal growth techniques were investigated: (i) VP ZnO single crystals grown via chemical vapor transport by Zn Technologies Inc. (USA); (ii) melt ZnO single crystals grown by high-pressure induction crystallization by Cermet Inc. (USA); and (iii) hydrothermal (HT) ZnO single crystals grown from supercritical aqueous solutions by Tokyo Denpa Co. Ltd. (Japan) [38–40].

As-grown ZnO single crystals are always n-type, irrespective of the growth method, and possess the highest reported electron mobilities for ZnO of $\sim 200\ cm^2\ V^{-1}\ s^{-1}$ due to their very high crystal quality with dislocation densities typically $\leqslant 10^4\ cm^{-2}$ [38]. Vapor-phase and melt ZnO have typical carrier concentrations of 10^{16}–$10^{17}\ cm^{-3}$ due to the unintentional incorporation of Al, Ga, In, and H shallow donors. In contrast, HT ZnO crystals are characterized by a much lower carrier concentration of 10^{13}–$10^{14}\ cm^{-3}$. This is attributed to a high degree of donor compensation by Li acceptors introduced from the Li_2CO_3 and LiOH mineralizers used to increase the solubility of ZnO. Other Group I impurities, such as Na and K, are also introduced but with approximately an order of magnitude lower concentration [38]. The relatively high concentration of Li impurities in HT ZnO (typically 10^{17}–$10^{18}\ cm^{-3}$) provides a significant point of difference compared to other ZnO material [38].

Consequently, we have also investigated HT ZnO single crystals from Tokyo Denpa Co. Ltd. (Japan) with reduced Li concentration that we will refer to as low-Li HT ZnO [41]. These low-Li HT ZnO crystals consist of conventional HT material that has been annealed at 1400 °C for 2 h to drive Li and other Group I impurities to the surface, where they are removed by subsequent regrinding and repolishing steps. This reduces the Li impurity concentration to 10^{14}–$10^{15}\ cm^{-3}$ and results in less-compensated material with carrier concentrations similar to that of VP and melt ZnO [41]. Since VP and melt ZnO should contain only trace amounts of Li, a comparative study involving both types of HT ZnO allows the role of Li in the PL of ZnO to also be investigated. This is important as Li can act as both a donor and acceptor in

ZnO and readily combines with hydrogen to form a range of defect complexes.

With respect to hydrogen incorporation, VP ZnO uses H_2 as a carrier gas to decompose the ZnO precursor material (at ∼1150 °C) and then transport it to a lower temperature growth zone. As such, VP ZnO typically contains the highest concentration of hydrogen impurities [38]. Hydrothermal ZnO also contains significant amounts of hydrogen due to its low temperature growth (300–400 °C) from a supercritical aqueous solution [40]. Melt ZnO is grown in a sealed high-pressure vessel at ∼1900 °C, where it is allowed to crystallize in an over-pressure of oxygen. Since no hydrogen-containing gases or solvents are used in the production of melt ZnO, it contains significantly less hydrogen than either VP or HT ZnO. Despite the high temperatures involved, some hydrogen present in the precursor material is incorporated into melt ZnO as it is grown in a closed system [39]. Low-Li HT ZnO contains the least amount of hydrogen as it is annealed (postgrowth) in an open system at 1400 °C, and no hydrogen-related defect complexes have been reported as being stable at this temperature [41].

ZnO single crystal wafers ($10 \times 10 \times 0.5\,\mathrm{mm}^3$) of each type were diced into nine equal-sized ($3 \times 3 \times 0.5\,\mathrm{mm}^3$) samples so that a complete annealing series could be carried out on material from the same wafer. Photoluminescence measurements at multiple positions across each wafer confirmed their excellent lateral homogeneity. Each sample was ultrasonically cleaned in organic solvents (acetone, methanol, and isopropanol) and dried in N_2 gas. In each case, the Zn-polar (0001) face was used because of its smoother surface morphology and lower defect density [42].

B. PL spectroscopy

All PL measurements were carried out at a temperature of 3 K in a reduced pressure helium flow cryostat (Oxford Optistat). The ZnO crystals were excited in a near-backscattering geometry ($\mathbf{E} \perp \mathbf{c}$ polarization) by the focused beam (using a single quartz lens) of the 325 nm (3.815 eV) line of a HeCd laser with a power of 15 mW (excitation power density of $\sim 10\,\mathrm{W/cm}^2$). Photoluminescence emission was detected in a ($\mathbf{E} \perp \mathbf{c}$, $\mathbf{k} \| \mathbf{c}$) geometry, where $\mathbf{E}$ is the electric field vector, $\mathbf{c}$ is directed along the (0001) c axis of the wurtzite ZnO crystal structure, and $\mathbf{k}$ is the wave vector. A Jobin-Yvon 1000M spectrometer with a focal length of 100 cm and a 1200-line/mm holographic grating was used to disperse the incoming PL emission. A cooled Hamamatsu R943-02 photomultiplier tube operating in photon counting mode was used for detection. Spectral resolution comfortably exceeded 100 μeV at the operating spectrometer slit widths. The sampling step size was chosen to be 50 μeV for most of the near band edge (NBE) region with finer steps of 10 μeV for the donor-bound excitons, allowing their relative emission energies to be determined to at least ± 20 μeV.

As the donor-bound-exciton region of ZnO PL is rich in closely spaced transitions—see for example the work of Meyer *et al.* [36] and Fig. 1 here—precise wavelength comparisons were required to understand the spectra from the wide range of ZnO single crystal samples studied. For each experiment, the sharp atomic transitions of a low-pressure Hg lamp were used for wavelength calibration via comparison

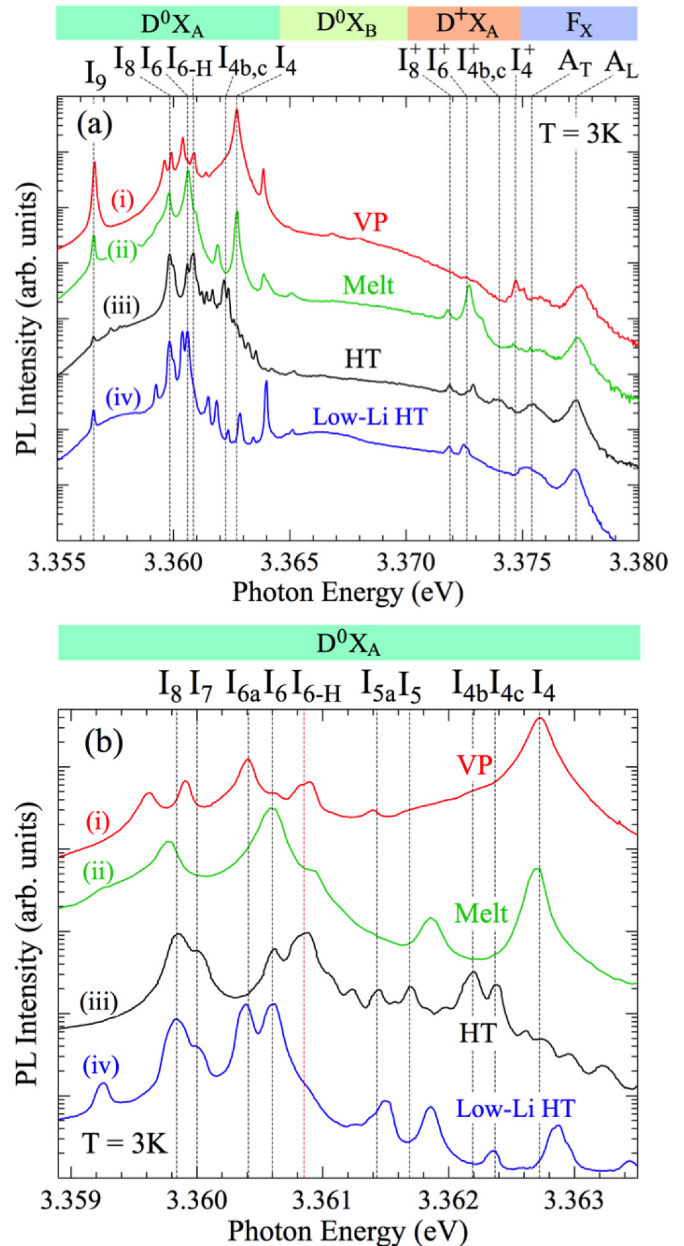

FIG. 1. (a) NBE PL spectra of four different types of ZnO single crystals at 3 K: (i) VP ZnO, (ii) melt ZnO, (iii) HT ZnO, and HT ZnO with low lithium concentration (low-Li HT ZnO); (b) neutral donor-bound exciton (D^0X_A) region for each of the four crystals. The Zn-polar (0001) face was investigated in all cases. The spectra have been vertically displaced for clarity.

with tabulated values of wavelength in vacuum [National Institute of Standards and Technology (NIST) Atomic Spectra Database]. From this comparison, the wavelength-dependent refractive index of air (n_{air}) in the UV region was determined and used to convert the measured PL emission wavelengths (λ_{air}) to vacuum photon energies (using $E = hc/n_{\mathrm{air}}\lambda_{\mathrm{air}}$). Repeated measurements on the same single crystal reference sample over multiple days indicated an absolute calibration accuracy of ±50 μeV. Wherever possible, PL measurements were performed on samples mounted on the same aluminum sample holder with the samples measured consecutively during

the same experimental run. The samples were mounted to the holder using silver colloidal paste at room temperature, employing surface tension for adhesion so that strain was not introduced. An as-received single crystal ZnO reference sample of each type was also repeatedly mounted in the cryostat alongside the corresponding processed samples in order to provide a consistent reference spectrum for the comparison of spectra taken during different experiments.

C. Annealing and ion implantation

Annealing studies were performed on $3 \times 3 \times 0.5\,\mathrm{mm}^3$ samples of each type of bulk ZnO single crystal in a quartz furnace tube in the presence of flowing O_2 or N_2 gas at 600 °C for 90 min or in flowing FG (5% H_2/95% N_2) at 600 °C for 60 min. A FG mixture of 5% H_2/95% Ar was also used to rule out the influence of nitrogen incorporation in any of the hydrogen-related features introduced by FG annealing.

Hydrogen and deuterium ion implantation was carried out on samples from the same wafer at the National Isotope Centre at GNS Science (Lower Hutt, New Zealand) under normal incidence with fluences of 7×10^{14} and $7 \times 10^{15}\,\mathrm{ions\,cm^{-2}}$. Theoretical implantation profiles were calculated via Transport of Ions in Matter (TRIM) simulations to achieve a boxlike implantation depth centered at 20 nm beneath the surface using multiple implantation energies between 4–18 keV [43,44]. The samples were implanted at room temperature under ultra-high vacuum conditions with an ion current of $<0.1\ \mu$A, using raster scanning to produce a laterally homogeneous implantation. The implanted samples were annealed in 100 °C steps at temperatures from 200 to 600 °C for 30 min per step in a flowing O_2 atmosphere, with PL spectra measured after each annealing step. As well as introducing higher concentrations of hydrogen into the samples, the implantation process also creates a higher density of intrinsic defects. The subsequent stepwise annealing process has the dual effect of gradually increasing the mobility of the implanted hydrogen, thereby allowing it to be captured by the introduced defects, while also gradually repairing the implantation damage.

III. RESULTS

A. As-received ZnO single crystals

Figure 1(a) shows the NBE PL of the four different ZnO single crystals. All spectra were taken at 3 K from the Zn-polar (0001) face, and the most prominent features have been labeled using the line notation introduced by Reynolds *et al.* [35] and further expanded by Meyer *et al.* [36] The NBE region contains the radiative recombination of *A*- and *B*-valence band excitons bound to neutral donors (D^0X_A and D^0X_B, respectively), *A*-valence band excitons bound to ionized donors (D^+X_A), and the longitudinal (A_L) and transversal (A_T) free excitons (F_X). The donor origin of the D^0X_A recombination lines I_6 (3.36060 eV), I_8 (3.35984 eV), and I_9 (3.35657 eV) have been identified using ion implantation and radio-tracer experiments as due to substitutional Al, Ga, and In (on the Zn site), respectively [36,45]. These are usually the most common nonhydrogenic impurities in ZnO, and the corresponding D^0X_A lines were present in all four ZnO crystals, as shown in Fig. 1(a). Surprisingly, the commonly reported H_O-related I_4 line (3.36272 eV) was only present in VP and melt ZnO and was completely absent in HT ZnO. The very high intensity of the I_4 line in VP ZnO is expected as H_2 gas is directly used in the growth of this material. The lower intensity of I_4 in melt ZnO is not surprising given that this material is grown without the use of hydrogen-containing processing gases or solvents, with hydrogen just introduced from the precursor material.

Figure 1(b) shows the D^0X_A region in greater detail, revealing the fine structure of the Al-related I_6 emission. Three different recombination lines can be observed in the vicinity of I_6 (3.36060 eV) depending on the ZnO material. In HT ZnO, a previously unreported line labeled as $I_{6\text{-}H}$ (3.36085 eV) that we will show (using FG annealing and H/D implantation experiments) is hydrogen related, can be clearly resolved on the high energy side of I_6. Here, $I_{6\text{-}H}$ also appears to be present at a much lower intensity in VP ZnO, in which I_{6a} (3.36041 eV) seems to be the dominant Al-related recombination line. In low-Li HT ZnO, both I_6 and I_{6a} were observed, whereas for melt ZnO, only I_6 was present. The presence or absence of these close lying recombination lines is likely to be related to different concentrations and configurations of Al impurities introduced by the different growth processes and growth temperatures for these ZnO materials.

The absence of the H_O-related I_4 (3.36272 eV) line in HT ZnO is surprising. Hydrothermal ZnO is known to contain significant concentrations of hydrogen due to its growth from a supercritical aqueous solution [38,40]. In place of I_4, a doublet $I_{4b,c}$ consisting of two closely lying recombination lines, I_{4b} (3.36219 eV) and I_{4c} (3.36237 eV), was observed in HT ZnO that we will also show is hydrogen related. Since Meyer *et al.* [36] have already assigned an unknown transition at 3.3620 eV as I_{4a}, our assignment will use I_{4b} and I_{4c} to maintain consistency with their notation. A strain-related effect is unlikely to be responsible for the energetic difference between the conventional I_4 line and the new $I_{4b,c}$ doublet, as all other recombination lines showed no shift in their expected position. Neither I_4 nor I_{4b} was present in low-Li HT ZnO, although there was a small residual emission peak at the energetic position of I_{4c}. This suggests that the donor responsible for I_{4b} has been removed by the high-temperature annealing (1400 °C) process used in the production of low-Li HT ZnO.

Temperature-dependent PL measurements (3 to 300 K) were performed on HT ZnO to determine whether the hydrogen-related recombination lines $I_{6\text{-}H}$ (3.36085 eV), I_{4b} (3.36219 eV), and I_{4c} (3.36237 eV) involve ground or excited excitonic states. The intensities of these recombination lines versus temperature are shown in the Arrhenius plots of Fig. 2, alongside that of the Al donor-related I_6 recombination line for comparison. The peak intensities of I_6 and $I_{6\text{-}H}$ decrease monotonically with increasing temperature, a behavior typical of donor-bound excitons in their ground state [46,47]. The solid lines in Fig. 2 represent fits to the data from which the decay and activation energies were obtained, following the procedure described by Shibata [48]. In the case of I_{4b}, a decrease in intensity with increasing temperature was observed, indicating a ground state, whereas I_{4c} showed an initial increase in intensity, suggesting that it may involve an excited state, although the effect is relatively small compared to that reported by Meyer *et al.* [46] for other known excited states.

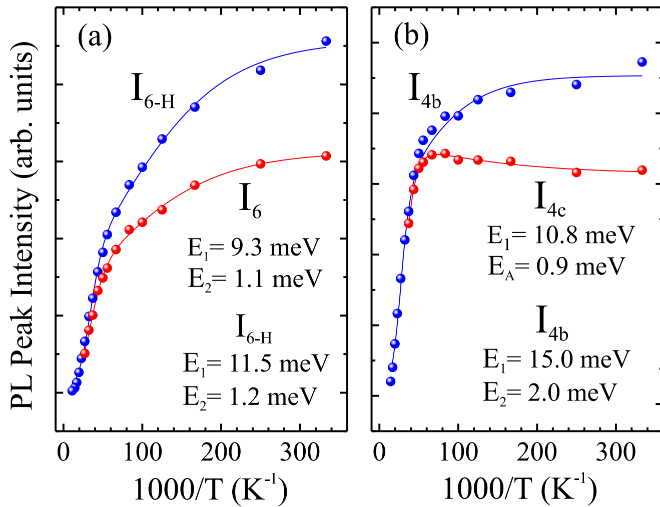

FIG. 2. Arrhenius plots of (a) the recombination lines I_6 and $I_{6\text{-}H}$ and (b) the recombination lines I_{4b} and I_{4c} of HT ZnO. Dots are the experimental peak intensities, and the solid lines are the fits to the data with the corresponding decay energies E_i and activation energy E_A [note: the intensity scaling of panel (a) is 2.5 times that of panel (b)].

B. Annealing HT ZnO in different atmospheres

Figure 3 shows the results of an annealing study performed on samples from the same HT-ZnO single crystal. Two samples were separately annealed, one in N_2 and the other in O_2 at 600 °C, with the O_2 annealed sample subsequently annealed at 600 °C in FG, followed by a second 600 °C anneal in O_2. Figure 3(a) shows the entire NBE region, while Fig. 3(b) shows the D^0X_A emission in greater detail. A remarkable decrease in the background intensity of the NBE emission between 3.363 and 3.372 eV was observed after annealing in both N_2 and O_2 ambients, revealing a host of previously obscured features [Fig 3(a): spectra (ii) and (iii)]. Of these, the transitions I_8^B (3.36435 eV), I_6^B (3.36496 eV), and $I_{6\text{-}H}^B$ (3.36520 eV) are attributed to neutral donor-bound excitons that involve a hole from the B-valence band. The energetic separation of ∼4.4 meV above their respective ground states (the A-valence band transitions I_8, I_6, and $I_{6\text{-}H}$) is in good agreement with the theoretical A-B valence band splitting [36,49]. The decrease in background intensity also allows the ionized donor-bound exciton emission (D^+X_A) to be resolved in greater detail, and the closely spaced I_6^+ (3.37261 eV) and $I_{6\text{-}H}^+$ (3.37291 eV) recombination lines can now be separately identified [Fig 3(a): spectrum (ii)].

Significant differences can be seen in the evolution of the new hydrogen-related lines $I_{6\text{-}H}$ (3.36085 eV), I_{4b} (3.36219 eV), and I_{4c} (3.36237 eV) on annealing in different atmospheres that provides an insight into their origins, as shown in Figs. 3(a) and 3(b). In particular, $I_{6\text{-}H}$ was almost unaffected by annealing at 600 °C in N_2 gas [spectrum (ii)], while $I_{6\text{-}H}$ and its excited state transitions $I_{6\text{-}H}^B$ and $I_{6\text{-}H}^+$ were completely removed by annealing at the same temperature in O_2 gas [spectrum (iii)]. Here, $I_{6\text{-}H}$ could be subsequently reintroduced by a 600 °C FG anneal [spectrum (iv)], and then removed again by a further 600 °C anneal in O_2 [spectrum (v)]. The reintroduction of $I_{6\text{-}H}$ by FG annealing and the observation that $I_{6\text{-}H}$ could only be removed by annealing in

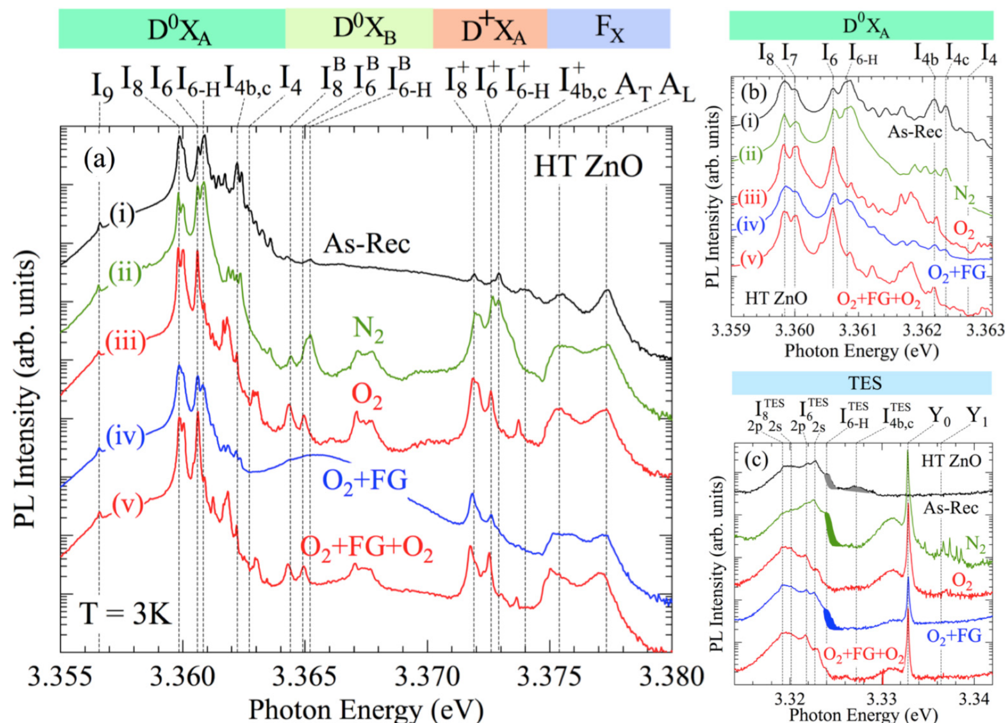

FIG. 3. (a) NBE 3 K PL spectra of HT ZnO single crystals after annealing at 600 °C in different atmospheres: (i) as-received, (ii) N_2 (90 mins), (iii) O_2 (90 mins), (iv) O_2 (90 mins) followed by FG (60 mins), and (v) O_2 (90 mins) followed by FG (60 mins) followed by O_2 (60 mins); (b) neutral donor-bound exciton (D^0X_A) region for each of the annealing conditions; and (c) TES region for each of the annealing conditions. The Zn-polar (0001) face was investigated in all cases. The spectra have been vertically displaced for clarity.

O_2, and not N_2, suggests the involvement of both hydrogen and oxygen vacancies in $I_{6\text{-}H}$. Note: the 600 °C FG annealing step [spectrum (iv)] was repeated using both (5% H_2/95% N_2) and (5% H_2/95% Ar) FG mixtures with no significant difference in the resulting spectra, ruling out the influence of nitrogen incorporation in $I_{6\text{-}H}$. Interestingly, the adjacent I_6 emission and its associated transitions (I_6^B and I_6^+) were largely unaffected by 600 °C annealing in any of the above ambients.

In contrast, the $I_{4b,c}$ doublet was removed by 600 °C annealing in both N_2 and O_2 atmospheres, although with some residual $I_{4b,c}$ emission in the case of N_2 annealing [see spectra (ii), (iii)]. Stepwise annealing at 50 °C increments in O_2 gas of a similar HT ZnO sample (not shown) showed that $I_{4b,c}$ anneals out at 400 °C, significantly lower than the H_O-related I_4 line observed in VP and melt ZnO that is usually removed at ~600 °C [36,50]. As I_{4b} and I_{4c} are unstable above 400 °C, the incorporation of hydrogen via 600 °C FG annealing only produced a slight recovery in their intensity [spectrum (iv)], especially compared to $I_{6\text{-}H}$, which was strongly reintroduced and therefore must have a higher thermal stability. Interestingly, the H_O-related I_4 line was not created by the FG annealing of HT ZnO, indicating that either an insufficient density of V_O sites were available or that $I_{6\text{-}H}$ and I_{4b}, I_{4c} were preferentially formed.

The large decrease in the broad background intensity of the NBE emission between 3.363 and 3.372 eV after 600 °C annealing in both N_2 and O_2 atmospheres was reversed by the 600 °C FG anneal [Fig. 3(a) spectrum (iv)]. This introduced a broad emission band centered at 3.366 eV that could again be removed by a second 600 °C O_2 anneal and subsequently reintroduced by another FG anneal. Separate experiments (not shown) involving PL from HT ZnO, measured through thin (~5 nm) radiofrequency (rf)-sputtered iridium oxide overlayers (deposited at room temperature) that also removed the same emission band, showed that this broad emission comes from the near-surface region of ZnO. It is also very similar in energy to the broad surface-related exciton feature reported in ZnO nanostructures [51,52]. It is therefore likely that this broad feature is linked to excitons bound to near-surface hydrogen that can be reversibly removed and reintroduced by annealing in different atmospheres.

Figure 3(c) shows the two electron satellite (TES) transitions of the A-valence band neutral donor-bound excitons (D^0X_A). The recombination of a neutral donor-bound exciton can leave the donor in the $1s$ ground state or in an excited $2s$ or $2p$ state. These $2s$ and $2p$ states can be resolved for the donor-bound excitons I_6 ($2s$: 3.3227 eV and $2p$: 3.3218 eV) and I_8 ($2s$: 3.3202 eV and $2p$: 3.3192 eV). Significantly, a distinct shoulder (colored area) on the high energy side of $I_6^{\mathrm{TES}}(2s)$ at 3.3240 eV was observed that correlates with the presence of the $I_{6\text{-}H}$ line in the sample. Like the $I_{6\text{-}H}$ line, this shoulder anneals out after 600 °C in O_2, but not N_2 gas, and reappears after 600 °C FG annealing. This correlation was consistently observed in several other HT ZnO samples, and therefore this shoulder is assigned to the TES of $I_{6\text{-}H}$. Similarly, a weak but reproducible feature was observed at 3.3272 eV in as-received HT ZnO (also consistently observed in other HT ZnO samples) that annealed out in both N_2 and O_2 atmospheres in the same way as $I_{4b,c}$, and consequently, this transition is assigned to the TES of $I_{4b,c}$.

Apart from these TES transitions, a comparatively very narrow and intense recombination line Y_0 (3.33282 eV) and an associated broad emission hump (on its low-energy shoulder) that scales with the intensity of Y_0 appeared in HT ZnO after 600 °C annealing in either N_2 or O_2 atmospheres [Fig. 3(c)]. It is known that, Y_0 and another sharp emission line Y_1 (3.33641 eV) observed in melt ZnO (and epitaxial ZnO films) originate from the radiative recombination of excitons bound to extended structural defects [53]. Here, stepwise annealing at 50 °C increments in O_2 gas (30 min per step) on similar HT ZnO samples (not shown) showed that Y_0 emerges at temperatures between 450-500 °C. Figure 3(c) shows that although Y_0 is not removed by 600 °C FG annealing, its intensity does appear to decrease and is increased again following a second 600 °C O_2 gas anneal. Although not conclusive, this behavior suggests that hydrogen may have a passivating effect on the associated extended structural defect.

C. Annealing VP, melt, and low-Li ZnO in different atmospheres

For comparison, we also annealed VP ZnO, melt ZnO, and low-Li HT ZnO at 600 °C in different atmospheres, and the resulting D^0X_A and TES PL is shown in Fig. 4. For VP ZnO, both $I_{6\text{-}H}$ and I_4 were removed by the 600 °C O_2 anneal, but only I_4 was reintroduced by annealing in FG [Fig. 4(a)]. Significantly, $I_{6\text{-}H}$ was not reintroduced by the FG annealing of VP ZnO, as it was in HT ZnO, indicating that a different nonhydrogen-related recombination may occur at the same energy as $I_{6\text{-}H}$ in VP ZnO. The I_4 line in melt ZnO was also removed and then reintroduced after 600 °C annealing in O_2 and FG, respectively, but again no $I_{6\text{-}H}$ emission was observed [Fig. 4(c)]. Neither I_{4b} nor I_{4c} was introduced into VP ZnO or melt ZnO by FG annealing.

In the case of low-Li HT ZnO, 600 °C annealing in O_2 (not shown) had little effect as this material has already been annealed at 1400 °C for 2 h in its production. However, the $I_{6\text{-}H}$ line was introduced by the 600 °C FG annealing of low-Li HT ZnO (using both H_2/N_2 and H_2/Ar), although at a lower intensity than in HT ZnO [see Fig. 4(e)]. The fact that $I_{6\text{-}H}$ can be reintroduced into both HT ZnO and low-Li HT ZnO by FG annealing, but not into VP ZnO or melt ZnO, indicates that the donor complex responsible for $I_{6\text{-}H}$ is related to impurities uniquely present in HT ZnO material.

D. Hydrogen and deuterium implantation

To further explore the nature of the hydrogen-related excitons $I_{6\text{-}H}$ and $I_{4b,c}$, hydrogen (H) and deuterium (D) ions were implanted at room temperature into HT ZnO and low-Li HT ZnO single crystals at doses of 7×10^{14} and 7×10^{15} ions cm^{-2}. Following implantation, the crystals were stepwise annealed in O_2 gas from 200 to 600 °C at 100 °C intervals. The PL spectra (and the changes on annealing) for both doses were very similar, and the D^0X_A spectra for the 7×10^{14} ion cm^{-2} dose are shown in Fig. 5, with the exception of the H-implanted HT ZnO sample for which the thermal evolution of the new features following the 7×10^{15} cm^{-2} dose was slightly clearer. Figure 5(a) and 5(b) shows the D^0X_A spectra for H- and D-implanted HT ZnO, respectively, after each annealing step. After ion implantation,

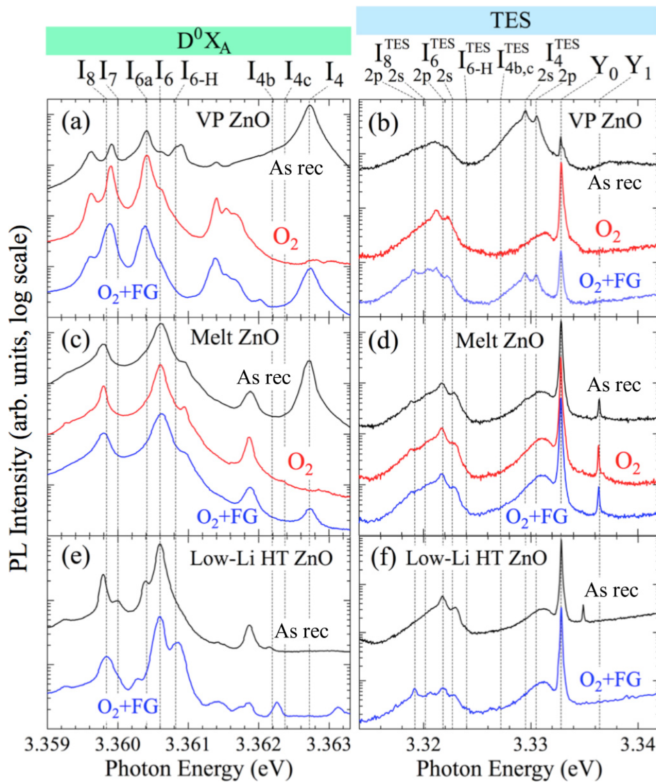

FIG. 4. 3 K PL spectra of the neutral donor-bound exciton (D^0X_A) region and the TES region of (a) and (b) VP ZnO, (c) and (d) melt ZnO, (e) and (f) HT ZnO with low lithium concentration (low-Li HT ZnO) before and after annealing at 600 °C in O_2 (90 mins), and O_2 (90 mins) followed by FG (60 mins). The Zn-polar (0001) face was investigated in all cases. The spectra have been vertically displaced for clarity.

the D^0X_A emission showed a general decrease in intensity and peak broadening due to the introduction of structural defects and the creation of nonradiative recombination centers by the implantation process. In both H- and D-implanted samples, a broad feature at 3.36272 eV appeared at the same energetic position as the H_O-related I_4 line that is not usually present in HT ZnO. It is therefore likely that both H and D implantation into HT ZnO leads to the preferential incorporation of hydrogen in the I_4 configuration (i.e. H_O) in contrast to the $I_{4b,c}$ (3.36219, 3.36237 eV) configuration usually observed in unimplanted HT ZnO [see the unimplanted reference spectrum in Figs. 5(a) and 5(b)]. After annealing at 400 °C, the I_4 line disappeared, and emission lines appeared at the usual $I_{4b,c}$ energetic positions. There was no observed isotope shift in the energetic position of the $I_4/I_{4b,c}$ emission (H versus D) and no local mode phonon replicas of $I_4/I_{4b,c}$, that might show an isotope shift, were detected.

Surprisingly, in H- and D-implanted HT ZnO, $I_{6\text{-}H}$ was still present after 600 °C O_2 annealing, although its relative intensity compared to I_6 decreases above 400 °C. This is in contrast to the behavior of unimplanted samples in which $I_{6\text{-}H}$ was removed by 600 °C O_2 annealing [Fig. 3(a)]. However, Ip *et al.* [54] also reported a higher thermal stability for hydrogen incorporated by ion implantation, due to increased trapping at residual damage. The temperature stability of the I_4 and $I_{6\text{-}H}$ peaks was remarkably consistent for both hydrogen and deuterium implantation, despite their mass difference.

The D^0X_A spectra for H- and D-implanted low-Li HT ZnO are shown in Fig. 5(c) and 5(d). The H_O-related I_4 line (not previously present) was again observed after implantation and disappeared after annealing at 400 and 500 °C, respectively. After implantation, $I_{6\text{-}H}$ was introduced in low-Li HT ZnO (although also not previously present), and this also annealed out at 400 and 500 °C for H and D implantation, respectively.

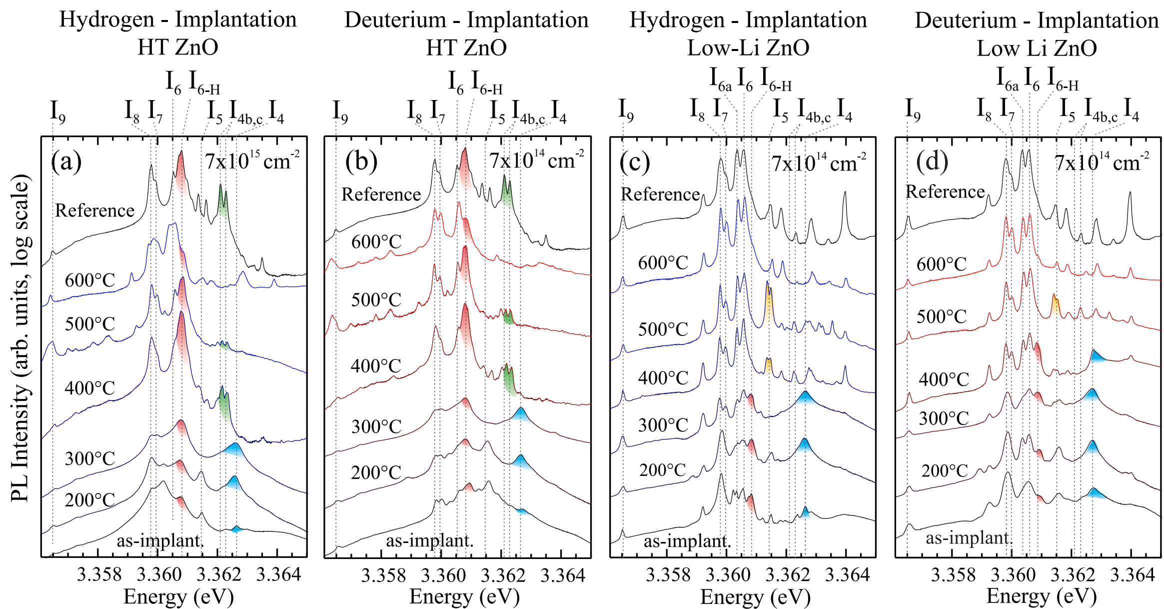

FIG. 5. 3 K PL spectra of the neutral donor-bound exciton (D^0X_A) region of HT ZnO before and after implantation (and subsequent 30 min annealing steps in O_2 gas from 200 to 600 °C) with (a) hydrogen and (b) deuterium; and the same experiment repeated for low-Li HT ZnO with (c) hydrogen and (d) deuterium implantation. All spectra were taken from the Zn-polar (0001) face of samples of the same wafer. The spectra have been vertically displaced for clarity.

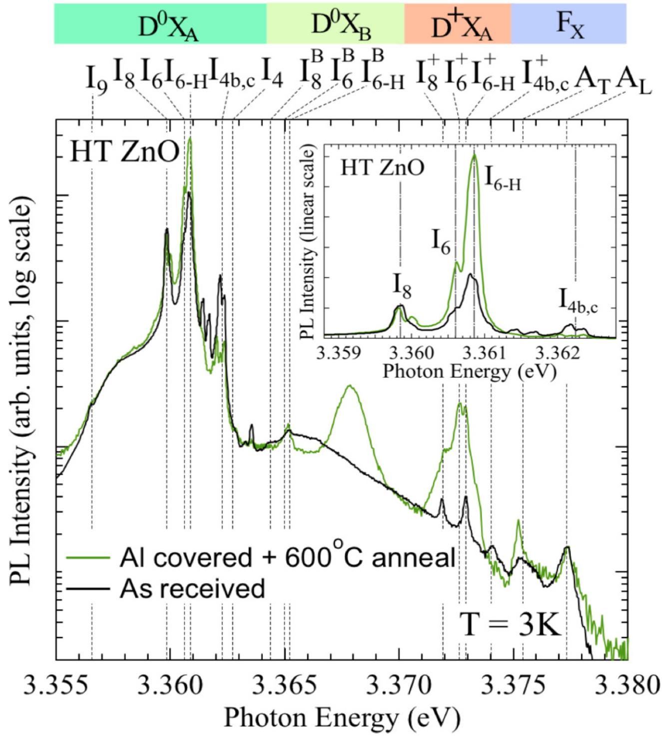

FIG. 6. NBE 3 K PL spectra of HT ZnO before and after coverage with a thin (∼10 nm) layer of aluminum followed by 30 min annealing at 600 °C in N_2. The inset shows the neutral donor-bound exciton (D^0X_A) region in greater detail using a linear scale. The spectra were taken from the Zn-polar (0001) face of the same wafer.

The Al-related emission line I_{6a} (3.36041 eV) observed in low-Li HT ZnO but not HT ZnO was unaffected by heat treatment. However, another new recombination line I_5 (3.36143 eV) was introduced into both HT ZnO and low-Li HT ZnO by H and D implantation, but this disappeared after annealing at just 300 °C. However, in the case of implanted low-Li HT ZnO only, this I_5 line reappeared after 400 °C annealing in the form of a doublet (3.36137, 3.36148 eV), with a fine splitting of just 110 μeV that reached a remarkably strong intensity after the 500 °C anneal before disappearing again after annealing at 600 °C.

E. Aluminum coverage and N_2 annealing

The location of $I_{6\text{-}H}$ on the high-energy shoulder of the well-known Al_{Zn}-related I_6 line suggests the possible involvement of Al in the defect complex responsible for $I_{6\text{-}H}$. To test this hypothesis, the Zn-polar face of another HT ZnO sample was covered with a thin (∼10 nm) layer of Al, deposited at room temperature via dc sputtering, that was then annealed for 30 min at 600 °C in N_2 gas to diffuse the Al into the sample (note: $I_{6\text{-}H}$ was earlier shown to be stable against N_2 annealing at this temperature). Figure 6 shows the NBE PL spectra of the HT ZnO sample before and after Al coating and 600 °C N_2 annealing. This clearly shows a large increase in the intensity of both I_6 and $I_{6\text{-}H}$ and also the corresponding ionized donor-bound emission I_6^+ and $I_{6\text{-}H}^+$ in the HT ZnO sample after Al coating and annealing, confirming the involvement of Al in I_6 and $I_{6\text{-}H}$. The other noticeable change was the large reduction in $I_{4b,c}$ although this is not surprising since it has already been shown that this hydrogen-related doublet is not thermally stable at 600 °C in either N_2 or O_2 atmospheres.

IV. DISCUSSION

In this paper, FG annealing and H and D implantation were used to identify two new hydrogen-related excitons $I_{4b,c}$ and $I_{6\text{-}H}$, in the low-temperature PL spectra of HT ZnO, with a third feature I_5 also very likely related to hydrogen. Table II summarizes the energies of the hydrogen-related exciton transitions in ZnO (highlighted in gray) and the binding energy of the corresponding donor. The donor binding energy was obtained from the $1s$-$2p$ energetic separation between the neutral donor-bound exciton recombination (D^0X_A) and its corresponding TES transition [shown in Figs. 3(c), and Figs. 4(b), 4(d), and 4(f)] using the effective mass approximation and applying the corrections proposed by Meyer *et al.* [36] for the effects of anisotropy and polaron interactions. In each case, the localization energies are given from the transverse

TABLE II. Energies of the PL transitions of the hydrogen-related (highlighted in gray) donor-bound excitons I_4 to $I_{6\text{-}H}$ and their associated excited states compared to those of substitutional Al (I_6, I_{6a}), Ga (I_7), and In (I_9): $D^0X_AE(1s)$ is the recombination energy of the neutral donor-bound A-valence band exciton in its $1s$ ground state, E_{loc} is its localization energy with reference to A_T, E_D is the donor binding energy, TES($2p$) is the energy of the TES in the $2p$ excited state, E($1s$-$2p$) is the energetic separation between D^0X_A and TES($2p$), D^0X_B, is the energy of neutral donor bond exciton involving a B-valence band hole, and D^+X_A is the energy of the A-valence band exciton bound to an ionized donor.

Exciton	D^0X_AE ($1s$) (eV)	E_{loc} (meV)	E_D (meV)	TES ($2p$) (eV)	E ($1s$-$2p$) (meV)	D^0X_B (eV)	D^+X_A (eV)	Assignment
I_4	3.36272	12.68	45.8	3.3295	33.2		3.37470	H_O
I_{4c}	3.36237	13.03	47.7	3.3272	35.1	3.3665	3.3740	Li_{Zn}-H_O
I_{4b}	3.36219	13.21						
I_5	3.36143	13.97	49.1[a]	—	—	—	3.37373	V_O-H_3
$I_{6\text{-}H}$	3.36085	14.55	49.5	3.3240	36.9	3.36520	3.37291	Al_{Zn}-H_O-Li_{Zn}
I_6	3.36060	14.80	51.4	3.3218	38.8	3.36496	3.37261	Al_{Zn}
I_{6a}	3.36041	14.99	51.8	3.3212	39.2	—	3.37261	Al_{Zn}
I_8	3.35984	15.56	53.2	3.3192	40.6	3.36435	3.37189	Ga_{Zn}
I_9	3.35657	18.83	63.5	3.3057	50.9	—	3.36874	In_{Zn}

[a]The value of E_D for I_5 has been estimated using Haynes' rule.

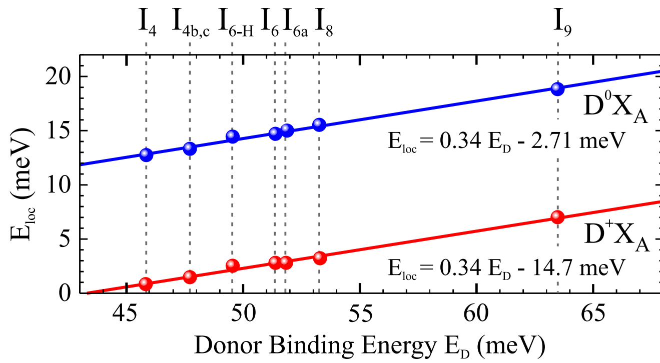

FIG. 7. Localization energy (E_{loc}) of the neutral (D^0X_A) and ionized (D^+X_A) donor-bound excitons in ZnO as a function of the donor binding energy (E_D). The respective energy values for $I_{4b,c}$, $I_{6\text{-}H}$, I_6, and I_8 were determined from HT ZnO, while I_4, I_{6a}, and I_9, were determined from VP ZnO samples.

free exciton ($A_T = 3.37540$ eV). The energies of the dominant nonhydrogenic I_6 (Al_{Zn}), I_8 (Ga_{Zn}), and I_9 (In_{Zn}) donor-bound excitons, determined from the PL measurements in this paper, are also listed for comparison.

Figure 7 shows the localization energies for the neutral (D^0X_A) and ionized donor-bound (D^+X_A) excitons as a function of their donor binding energy. The linear relationship for the D^0X_A excitons is known as Haynes' rule [55]. This relationship was shown by Meyer *et al.* [46,56] to also apply for D^+X_A excitons. Linear fits to our experimental data (Fig. 7) yield $E_{\text{loc}} = 0.34E_D - 2.71$ meV for the D^0X_A excitons, similar to previously reported trends [36,56,57], and $E_{\text{loc}} = 0.34E_D - 14.7$ meV for the D^+X_A excitons. The common slopes indicate identical hole masses for the neutral

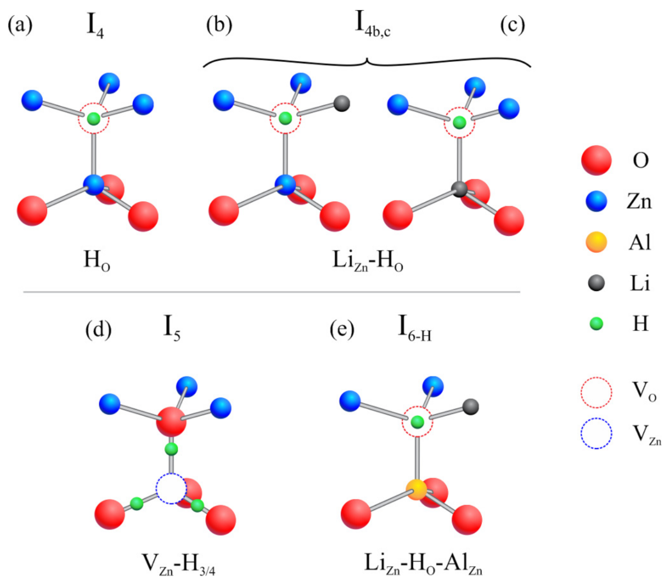

FIG. 8. Likely physical structures of the hydrogen-related defect complexes associated with the neutral donor-bound excitons I_4, $I_{4b,c}$, I_5, and $I_{6\text{-}H}$, observed in ZnO PL. (Note: the $I_{4b,c}$ defect structures shown would require an additional H atom in the Li_{Zn}-H-O configuration to act as an overall donor, rather than as a neutral donor-acceptor pair).

and ionized donor-bound excitons [46]. The newly identified hydrogen-related excitons $I_{6\text{-}H}$ and $I_{4b,c}$ lie close to both the D^0X_A and D^+X_A trend lines, confirming their assignment as due to shallow donors. (Note: the uncertainty in the position of the $I_{6\text{-}H}$ exciton is significantly larger than for the other data points in Fig. 7 due to the fact that the TES of $I_{6\text{-}H}$ could only be resolved as a shoulder on the high-energy side of $I_6{}^{\text{TES}}(2s)$, as shown in Fig. 3(c). This results in a higher uncertainty in the calculated value of E_D for $I_{6\text{-}H}$, which may explain the small deviation of $I_{6\text{-}H}$ from both trend lines). The D^0X_A relationship was also used to estimate a donor binding energy of 49.1 meV for the likely hydrogen-related I_5 exciton from its localization energy. For donor binding energies lower than 43.2 meV, an exciton cannot bind to the respective ionized donor, as its localization energy would approach zero. The location energy of I_4^+, obtained from the PL spectra of VP ZnO, is only 0.7 meV, as it is associated with the lowest binding energy hydrogen-related shallow donor.

We now discuss the assignment of the hydrogen-related excitons, $I_{4b,c}$, $I_{6\text{-}H}$, and I_5 and their correlation with previously identified hydrogen-related features observed in IR and Raman spectroscopy (see Table I). The most likely hydrogen-related defect complexes involved in $I_{4b,c}$, $I_{6\text{-}H}$, and I_5 are illustrated in Fig. 8. We also discuss the origin of the broad hydrogen-related NBE emission band between 3.363 and 3.372 eV.

A. $I_{4b,c}$ versus I_4

The most commonly observed hydrogen-related shallow donors in ZnO are bond-centered interstitial hydrogen (H_{BC}) and multicoordinated H bound inside an oxygen vacancy (H_O) [12]. It is known that, H_O has a significantly higher thermal stability (∼600 °C) than H_{BC} (⩽190 °C), which readily dissociates to form electrically inactive hydrogen molecules (i.e. H_2) [16,24]. Here, H_O with a donor binding energy of 45.8 meV is the main hydrogen-related contributor to the unintentional *n*-type conductivity of ZnO [10] and is also the origin of the widely reported I_4 recombination line at 3.3628 eV in ZnO PL [12,36]. However, in contrast to VP and melt ZnO that showed well-defined I_4 emission, no evidence of I_4 was found in HT ZnO. Instead, a doublet of two closely spaced recombination lines, $I_{4b,c}$ [I_{4b} (3.36219 eV), I_{4c} (3.36237 eV)] and their ionized donor (D^+X_A), *B*-exciton, and TES transitions were consistently observed in HT ZnO. Hydrothermally grown (HT) ZnO differs from other ZnO material in that it contains high concentrations of Li that readily forms complexes with hydrogen [38,40]. As this high-Li content is the outstanding difference between HT ZnO and other forms of ZnO, it is reasonable to assume that Li is involved in $I_{4b,c}$ and other hydrogen-related emission lines, such as $I_{6\text{-}H}$, that are unique to HT ZnO. Furthermore, Chan *et al.* [58] reported a striking correlation (both in terms of the shape and location) between the Li and H concentrations, measured using secondary ion mass spectrometry, in H-implanted HT ZnO after annealing at 600 °C in air. This correlation suggests that H is efficiently captured by Li-related defects in HT ZnO.

The most commonly reported Li-H defect complex in HT ZnO is the Li_{Zn}-H-O configuration involving a substitutional Li_{Zn} acceptor passivated by an OH group on an adjacent oxygen site. Halliburton *et al.* [20] used IR adsorption and

photoinduced electron paramagnetic resonance experiments to assign this complex to a 3577 cm^{-1} OH-vibrational line that is usually dominant in HT ZnO. Wardle *et al.* [59] used first-principles DFT calculations to show that the bond-centered H position is the lowest energy state, while Shi *et al.* [21] identified ^{6}Li and ^{7}Li isotope splitting in its deuterium (Li_{Zn}-D-O) counterpart. However, Lavrov *et al.* [22] showed that the 3577 cm^{-1} local vibrational mode in HT ZnO is very stable and can only be destroyed at a temperature of 1200 °C (for several hours) and therefore does not fit the thermal stability of $I_{4b,c}$ that we have shown can be annealed out at just 400 °C. Johansen *et al.* [23] proposed that the high thermal stability of Li_{Zn}-OH complexes was most likely due to the efficient recapturing of H by Li_{Zn} and showed that the 3577 cm^{-1} signal could be removed from HT ZnO by rapid cooling in deionized H_2O after annealing at 650 °C. However, the samples in this paper were slowly cooled in air after annealing, and under these conditions, the same authors observed that the 3577 cm^{-1} signal was present even after annealing at 1250 °C for 30 min.

The relatively close recombination energy of $I_{4b,c}$ (3.36219, 3.36237 eV) compared to the commonly observed H_O-related (3.36272 eV) neutral donor-bound exciton I_4, their similar donor binding energies of 45.8 and 47.7 meV, respectively, and the fact that they can both be removed by annealing in either N_2 or O_2 atmospheres (albeit at different temperatures of 400 and 600 °C, respectively) suggests a similar H_O origin, with a perturbation due to the presence of Li in HT ZnO. Vidya *et al.* [60] used first-principles DFT calculations to investigate complexes between Li and intrinsic defects in ZnO. They showed that the complex between Li_{Zn} and an adjacent oxygen vacancy (V_O) has a donor character and is energetically favorable in ZnO, with a lower formation energy than Li_{Zn} alone. Similar to the conversion of V_O to H_O, the hydrogenation of Li_{Zn}-V_O to form Li_{Zn}-H_O is likely to transform the V_O defect from a deep to a shallow donor state [10], and therefore $I_{4b,c}$ in HT ZnO is assigned to the Li_{Zn}-H_O complex [Figs. 8(b) and 8(c)]. Furthermore, the splitting of $I_{4b,c}$ (3.36219, 3.36237 eV) is likeky to correspond to the different position of the substitutional Li in the tetrahedral Zn nearest neighbor configuration of H_O, i.e. with the Li-H_O bond either parallel or nonparallel to the c axis.

The assignment of $I_{4b,c}$ to the Li_{Zn}-H_O complex explains why it partially reappeared after the 600 °C annealing in FG (either N_2-H_2 or Ar-H_2) of HT ZnO due to the reintroduction of hydrogen and the formation of new Li_{Zn}-V_O sites. It also explains the unusual behavior following the H and D implantation of HT ZnO, when I_4 was introduced but was only stable up to and including 300 °C O_2 annealing and was replaced after annealing at 400 °C by $I_{4b,c}$: The implantation process produces an increased concentration of V_O (via collision displacement) that can trap implanted hydrogen but also displaces substitutional Li_{Zn}. Børseth *et al.* [61] showed that Zn vacancy clusters formed by ion implantation damage can also trap displaced Li. Consequently, the majority of the as-implanted H will initially be trapped at newly created V_O sites that are not coordinated to a neighboring Li_{Zn} atom, explaining the observation of conventional H_O-related I_4 emission. On annealing, the removal of I_4 in HT ZnO is not just determined by the out-diffusion of hydrogen from H_O but also by the rate at which displaced Li atoms reoccupy vacant Zn lattice positions, with Li_{Zn}-V_O having a lower formation energy than Li_{Zn} [60]. This would explain the lower thermal stability of I_4 in implanted HT ZnO (300 °C) compared to other ZnO material (500–700 °C) and its replacement by $I_{4b,c}$ after 400 °C annealing. In H- and D-implanted low-Li HT ZnO, $I_{4b,c}$ was not observed after the removal of I_4, probably because of the significantly lower concentrations of Li_{Zn} present in this material.

The Li_{Zn}-H_O complex can be considered as a donor-acceptor pair with an overall neutral charge state. Therefore, in order to act as an overall shallow donor, the Li_{Zn} acceptor would need to be passivated by an additional H atom that is not shown in Figs. 8(b) and 8(c). As already discussed, the Li_{Zn}-H-O configuration involving a substitutional Li_{Zn} acceptor passivated by an OH group on an adjacent oxygen site is very stable in ZnO [22], and so it is possible that the Li_{Zn}-H_O complex is part of an overall O-H-Li_{Zn}-H_O configuration.

B. $I_{6\text{-}H}$ and I_6

In HT ZnO, a new (and usually dominant) hydrogen-related recombination line $I_{6\text{-}H}$ (3.36085 eV) located on the high-energy shoulder of the Al-related I_6 line (3.36060 eV) was identified. Although some low-intensity emission was observed at a similar energy in VP ZnO, this was not reintroduced by annealing in FG, and so this emission is most likely due to a different nonhydrogen-related feature. A possible candidate for this feature in VP ZnO is boron as this was detected by Avrutin *et al.* [38] in significant quantities in three VP ZnO samples from the same source (Zn Technologies, Inc.) as used here, but not in HT ZnO. Boron is a substitutional Group III donor impurity in ZnO (similar to the In_{Zn}, Ga_{Zn}, and Al_{Zn} donors that are responsible for the I_9, I_8, and I_6 emission lines, respectively) that would be expected, due to the empirical trend of decreasing localization energy with decreasing donor mass, to produce a D^0X_A emission line on the high-energy side of I_6. An alternative explanation is that $I_{6\text{-}H}$ is also present in VP ZnO, but is not reintroduced by FG annealing because the defect complex involved is present in significantly lower concentrations compared to HT ZnO.

However, the dominance of $I_{6\text{-}H}$ in HT ZnO and its reintroduction on FG annealing (either N_2-H_2 or Ar-H_2) does suggest the involvement of both Li and H in a defect complex. Furthermore, both the FG annealing of low-Li HT ZnO and its implantation with either H or D also introduced $I_{6\text{-}H}$ emission, albeit with a significantly lower intensity compared to HT ZnO due to its lower Li concentration. Here, $I_{6\text{-}H}$ could be removed from H/D implanted low-Li HT ZnO by annealing at 400/500 °C, compared to 600 °C in HT ZnO. This difference may be due to the fact that the distribution of Li (and therefore the distribution of $I_{6\text{-}H}$) is significantly more surface concentrated in low-Li HT ZnO compared to HT ZnO (due to its 1400 °C postgrowth heat treatment) [41], and therefore, the migration barrier for the loss of H/D from $I_{6\text{-}H}$ would be lower for low-Li HT ZnO.

Aluminum is also likely to be involved in $I_{6\text{-}H}$ due to its close proximity (∼0.2 meV) to the Al_{Zn}-related I_6 line and the fact both I_6 and $I_{6\text{-}H}$ were strongly enhanced by the coverage of HT ZnO with a thin (∼10 nm) layer of Al and subsequent

30 min annealing in N_2 at 600 °C. Significantly, $I_{6\text{-}H}$ completely disappeared after annealing as-received HT ZnO in O_2 at 600 °C but was unaffected by annealing in N_2 at the same temperature, which also indicates the involvement of oxygen vacancies. Together, these observations suggest that $I_{6\text{-}H}$ may originate from a defect complex involving Al, Li, H, and V_O. A possible model for this defect could be a Li_{Zn}-H_O-Al_{Zn} complex, as shown in Fig. 8(e). The donor binding energy of 49.5 meV for $I_{6\text{-}H}$ is close to the value of 48 meV determined by Look [62] using temperature-dependent Hall effect measurements for a possible $Al_{Zn} + Li_{Zn}$-H defect complex. Interestingly, $I_{6\text{-}H}$ is usually the dominant low-temperature PL emission line in HT ZnO, suggesting that the hydrogen-related defect responsible is present in significant concentrations.

C. I_5 and V_{Zn}-H_n

After H and D implantation, excitonic emission at the energetic position of I_5 (3.36143 eV) was created in HT ZnO and low-Li HT ZnO that disappeared after 300 °C O_2 annealing. Here, I_5 then reappeared in low-Li HT ZnO (but not HT ZnO) after 400–500 °C O_2 annealing, with a much stronger intensity and in the form of a doublet (3.36137, 3.36148 eV) that disappeared again at 600 °C. This intensity dependence with temperature is almost identical to that reported by Shi *et al.* [14,50] in both VP and melt ZnO for the IR absorption line at 3326 cm^{-1} that was identified as hydrogen related by McCluskey *et al.* [18] and can be formed via the thermal dissociation of hidden H_2 molecules [14]. Herklotz *et al.* [63] referred to the defect involved as XH while investigating hydrogenated melt ZnO and suggested a possible V_{Zn}-H model. Due to their very similar temperature dependence, it is likely that XH and I_5 have the same origin, and since VP and melt ZnO only contain trace amounts of Li, it is unlikely that Li is involved. Zhang *et al.* [29] observed a PL recombination line in hydrogen-implanted HT ZnO at 3.3617 eV (i.e. close to the energetic position of I_5) that appeared after 200 °C annealing in air but disappeared at 300 °C, which they proposed was due to the shallow donor V_{Zn}-H_3 involving three O-H bonds (a second smaller peak at 3.3610 eV was assigned to V_{Zn}-H_4). Here, I_5 disappeared at the same temperature but reappeared on 400–500 °C annealing in low-Li HT ZnO, but not HT ZnO. Johansen *et al.* [64] used positron annihilation spectroscopy to show that Li_{Zn} acts as the primary trapping site for hydrogen in HT ZnO, as the trapping efficiency of V_{Zn} is much lower in comparison. Consequently, V_{Zn}-H_n complexes will be more stable in low-Li HT ZnO as it contains significantly less Li_{Zn} to compete with their formation. Significantly, Johansen *et al.* [64] observed the formation of the neutral V_{Zn}-H_2 complex in Li-poor HT ZnO. It is therefore likely that I_5 is due to the recombination of excitons bound to a V_{Zn}-H_n complex [Fig. 8(d)], with the shallow donor V_{Zn}-H_3 the most likely candidate (although the involvement of V_{Zn}-H_4 cannot be ruled out) due to the energetic location of I_5 in the shallow neutral donor-bound exciton region of the ZnO PL spectrum.

D. Subsurface Hydrogen

A very broad NBE emission band from 3.363 and 3.372 eV was observed in HT ZnO that covered the entire region between the D^0X_A and D^+X_A emission. This band could be completely removed by either N_2 or O_2 annealing at 600 °C and subsequently reintroduced by FG annealing (either N_2-H_2 or Ar-H_2) at the same temperature. This removal/reintroduction process could be repeated multiple times on the same sample. Separate experiments (not shown) showed that the same band could also be completely removed by a very thin coating (∼5 nm) of iridium oxide (a material commonly used in the formation of high-quality Schottky contacts to ZnO) that was deposited by reactive rf sputtering at room temperature, as described elsewhere [65]. Significantly, the rest of the NBE emission was unaffected, suggesting that the band involves emission from the near-surface region of ZnO. It is also similar in energy and shape to a broad surface-related excitonic feature (referred to as S_x) reported in ZnO nanostructures [51,52]. Traeger *et al.* [66] quantified the hydrogen concentration profile in HT ZnO single crystals using ^{15}N nuclear reaction analysis and reported a significantly increased hydrogen concentration in the subsurface region (to ∼10 nm below the surface) of up to a factor of 10 compared to the bulk. They also observed that part of this subsurface hydrogen was less strongly bound and could be reversibly removed by heating to 550 °C and reintroduced by exposure to atomic hydrogen, similar to the behavior observed here. Consequently, the broad emission band from 3.363 and 3.372 eV is likely to involve some form of near-surface hydrogen.

V. CONCLUSIONS

In conclusion, several new hydrogen-related neutral donor-bound excitons and their *B*-exciton, ionized donor, and TES transitions have been identified in the PL of ZnO via a comparative study of four different types of bulk ZnO single crystal. Oxygen, nitrogen, and FG annealing were combined with hydrogen and deuterium implantation to determine the origin and temperature stability of these new hydrogen-related excitonic features. The hydrogen-related I_4 (3.36272 eV) emission commonly reported in vapor-phase and melt ZnO crystals was completely absent in HT ZnO and instead was replaced by a doublet of two closely lying recombination lines $I_{4b,c}$ (3.36219, 3.36237 eV) that were assigned to a Li_{Zn}-H_O defect complex with a donor binding energy of 47.7 meV. Another new hydrogen-related (and usually dominant) PL emission line $I_{6\text{-}H}$ (3.36085 eV) was also identified in HT ZnO in close proximity to the commonly observed Al-related I_6 line (3.36060 eV) and was associated with an Al_{Zn}-H_O-Li_{Zn} defect complex with a donor binding energy of 49.5 meV. A new doublet I_5 (3.36137, 3.36148 eV) also appeared in HT ZnO single crystals with low lithium concentrations after annealing at 400–500 °C, and this was associated with a V_{Zn}-$H_{3,4}$ defect complex with a donor binding energy of 49.1 meV. In addition, a broad NBE emission centered at 3.366 eV was associated with excitons bound to subsurface hydrogen. The identification of these new hydrogen-related excitonic features has important consequences for understanding and controlling the optoelectronic properties of ZnO materials.

ACKNOWLEDGMENTS

This paper was supported by the MacDiarmid Institute for Advanced Materials and Nanotechnology (Grant No. UOC 6360). M.W. Allen is the recipient of a Royal Society

of New Zealand Rutherford Discovery Fellowship (Grant No. RDF-UOC 1202). We acknowledge the assistance of P. Murmu at the National Isotope Centre at GNS Science, Lower Hutt, New Zealand.

[1] S. J. Pearton, J. W. Corbett, and T. S. Shi, Appl. Phys. A **43**, 153 (1987).
[2] J. Chevallier and M. Aucouturier, Ann. Rev. Mater. Sci. **18**, 219 (1988).
[3] S. K. Estreicher, Mater. Sci. Eng. R **14**, 319 (1995).
[4] S. J. Pearton, J. W. Corbett, and J. T. Borenstein, Physica B **170**, 85 (1991).
[5] C. G. Van de Walle and J. Neugebauer, Annu. Rev. Mater. Res. **36**, 179 (2006).
[6] C. G. Van de Walle and J. Neugebauer, Nature **423**, 626 (2003).
[7] C. G. Van de Walle, Phys. Rev. Lett. **85**, 1012 (2000).
[8] E. Mollwo, Z. Phys. **138**, 478 (1954).
[9] D. G. Thomas and J. J. Lander, J. Chem. Phys. **25**, 1136 (1956).
[10] A. Janotti and C. G. Van de Walle, Nat. Mater. **6**, 44 (2007).
[11] M. G. Wardle, J. P. Goss, and P. R. Briddon, Phys. Rev. Lett. **96**, 205504 (2006).
[12] E. V. Lavrov, F. Herklotz, and J. Weber, Phys. Rev. B **79**, 165210 (2009).
[13] E. V. Lavrov, F. Herklotz, and J. Weber, Phys. Rev. Lett. **102**, 185502 (2009).
[14] G. A. Shi, M. Saboktakin, M. Stavola, and S. J. Pearton, Appl. Phys. Lett. **85**, 5601 (2004).
[15] S. G. Koch, E. V. Lavrov, and J. Weber, Phys. Rev. Lett. **108**, 165501 (2012).
[16] S. G. Koch, E. V. Lavrov, and J. Weber, Phys. Rev. B **89**, 235203 (2014).
[17] F. Herklotz, E. V. Lavrov, V. Kolkovsky, J. Weber, and M. Stavola, Phys. Rev. B **82**, 115206 (2010).
[18] M. D. McCluskey, S. J. Jokela, K. K. Zhuravlev, P. J. Simpson, and K. G. Lynn, Appl. Phys. Lett. **81**, 3807 (2002).
[19] C. D. Corolewski, N. S. Parmar, K. G. Lynn, and M. D. McCluskey, J. Appl. Phys. **120**, 035703 (2016).
[20] L. E. Halliburton, L. J. Wang, L. H. Bai, N. Y. Garces, N. C. Giles, M. J. Callahan, and B. G. Wang, J. Appl. Phys. **96**, 7168 (2004).
[21] G. A. Shi, M. Stavola, and W. B. Fowler, Phys. Rev. B **73**, 081201(R) (2006).
[22] E. V. Lavrov, F. Börrnert, and J. Weber, Phys. Rev. B **71**, 035205 (2005).
[23] K. M. Johansen, H. Haug, E. Lund, E. V. Monakhov, and B. G. Svensson, Appl. Phys. Lett. **97**, 211907 (2010).
[24] S. G. Koch, E. V. Lavrov, and J. Weber, Phys. Rev. B **90**, 205212 (2014).
[25] E. V. Lavrov, J. Weber, F. Börrnert, C. G. Van de Walle, and R. Helbig, Phys. Rev. B **66**, 165205 (2002).
[26] F. Herklotz, A. Hupfer, K. M. Johansen, B. G. Svensson, S. G. Koch, and E. V. Lavrov, Phys. Rev. B **92**, 155203 (2015).
[27] J. K. Lee, M. Nastasi, D. W. Hamby, and D. A. Lucca, Appl. Phys. Lett. **86**, 171102 (2005).
[28] J. K. Dangbegnon, K. Talla, and J. R. Botha, Opt. Mater. **34**, 920 (2012).
[29] Z. Zhang, D. C. Look, R. Schifano, K. M. Johansen, B. G. Svensson, and L. J. Brillson, J. Phys. D: Appl. Phys. **46**, 055102 (2013).
[30] M. W. Allen, C. H. Swartz, T. H. Myers, T. D. Veal, C. F. McConville, and S. M. Durbin, Phys. Rev. B **81**, 075211 (2010).
[31] R. Heinhold, G. T. Williams, S. P. Cooil, D. A. Evans, and M. W. Allen, Phys. Rev. B **88**, 235315 (2013).
[32] R. Heinhold, S. P. Cooil, D. A. Evans, and M. W. Allen, J. Phys. Chem. C **118**, 24575 (2014).
[33] L. F. J. Piper, A. R. H. Preston, A. Fedorov, S. W. Cho, A. DeMasi, and K. E. Smith, Phys. Rev. B **81**, 233305 (2010).
[34] K. Ozawa and K. Mase, Phys. Rev. B **83**, 125406 (2011).
[35] D. C. Reynolds, C. W. Litton, and T. C. Collins, Phys. Rev. **140**, A1726, (1965).
[36] B. K. Meyer, H. Alves, D. M. Hofmann, W. Kriegseis, D. Forster, F. Bertram, J. Christen, A. Hoffmann, M. Strassburg, M. Dworzak, U. Haboeck, and A. V. Rodina, Phys. Status Solidi B **241**, 231 (2004).
[37] A. Teke, Ü. Özgür, S. Dogan, X. Gu, H. Morkoç, B. Nemeth, J. Nause, and H. O. Everitt, Phys. Rev. B **70**, 195207 (2004).
[38] V. Avrutin, G. Cantwell, J. Z. Zhang, J. J. Song, D. J. Silversmith, and H. Morkoc, Proç. IEEE **98**, 1339 (2010).
[39] J. Nause and B. Nemeth, Semicond. Sci. Tech. **20**, S45 (2005).
[40] K. Maeda, M. Sato, I. Niikura, and T. Fukuda, Semicond. Sci. Tech. **20**, S49 (2005).
[41] R. Heinhold, H. S. Kim, F. Schmidt, H. von Wenckstern, M. Grundmann, R. J. Mendelsberg, R. J. Reeves, S. M. Durbin, and M. W. Allen, Appl. Phys. Lett. **101**, 062105 (2012).
[42] M. W. Allen, R. J. Mendelsberg, R. J. Reeves, and S. M. Durbin, Appl. Phys. Lett. **94**, 103508 (2009).
[43] J. P. Biersack, Nucl. Instrum. Methods Phys. Res. B **27**, 21 (1987)
[44] J. Kennedy, D. A. Carder, A. Markwitz, and R. J. Reeves, J. Appl. Phys. **107**, 103518 (2010).
[45] K. Johnston, M. O. Henry, D. McCabe, E. McGlynn, M. Dietrich, E. Alves, and M. Xia, Phys. Rev. B **73**, 165212 (2006).
[46] B. K. Meyer, J. Sann, S. Eisermann, S. Lautenschlaeger, M. R. Wagner, M. Kaiser, G. Callsen, J. S. Reparaz, and A. Hoffmann, Phys. Rev. B **82**, 115207 (2010).
[47] R. J. Mendelsberg, M. W. Allen, S. M. Durbin, and R. J. Reeves, Phys. Rev. B **83**, 205202 (2011).
[48] H. Shibata, Jpn. J. Appl. Phys. **37**, 550 (1998).
[49] W. R. L. Lambrecht, A. V. Rodina, S. Limpijumnong, B. Segall, and B. K. Meyer, Phys. Rev. B **65**, 075207 (2002).
[50] G. A. Shi, M. Stavola, S. J. Pearton, M. Thieme, E. V. Lavrov, and J. Weber, Phys. Rev. B **72**, 195211 (2005).
[51] M. Biswas, Y. S. Jung, H. K. Kim, K. Kumar, G. J. Hughes, S. Newcomb, M. O. Henry, and E. McGlynn, Phys. Rev. B **83**, 235320 (2011).
[52] Y. Yang, B. K. Tay, X. W. Sun, J. Y. Sze, Z. J. Han, J. X. Wang, X. H. Zhang, Y. B. Li, and S. Zhang, Appl. Phys. Lett. **91**, 071921 (2007).
[53] M. R. Wagner, G. Callsen, J. S. Reparaz, J. H. Schulze, R. Kirste, M. Cobet, I. A. Ostapenko, S. Rodt, C. Nenstiel, M. Kaiser,

A. Hoffmann, A. V. Rodina, M. R. Phillips, S. Lautenschlager, S. Eisermann, and B. K. Meyer, Phys. Rev. B **84**, 035313 (2011).
[54] K. Ip, M. E. Overberg, Y. W. Heo, D. P. Norton, S. J. Pearton, C. E. Stutz, B. Luo, F. Ren, D. C. Look, and J. M. Zavada, Appl. Phys. Lett. **82**, 385 (2003).
[55] J. R. Haynes, Phys. Rev. Lett. **4**, 361 (1960).
[56] B. K. Meyer, J. Sann, S. Lautenschläger, M. R. Wagner, and A. Hoffmann, Phys. Rev. B **76**, 184120 (2007).
[57] A. Schildknecht, R. Sauer, and K. Thonke, Physica B **340**, 205 (2003).
[58] K. S. Chan, L. Vines, K. M. Johansen, E. V. Monakhov, J. D. Ye, P. Parkinson, C. Jagadish, B. G. Svensson, and J. Wong-Leung, J. Appl. Phys. **114**, 083111 (2013).
[59] M. G. Wardle, J. P. Goss, and P. R. Briddon, Phys. Rev. B **71**, 155205 (2005).
[60] R. Vidya, P. Ravindran, and H. Fjellvåg, J. Appl. Phys. **111**, 123713 (2012).
[61] T. M. Børseth, F. Tuomisto, J. S. Christensen, W. Skorupa, E. V. Monakhov, B. G. Svensson, and A. Y. Kuznetsov, Phys. Rev. B **74**, 161202(R) (2006).
[62] D. C. Look, Superlatt. Microstruct. **42**, 284 (2007).
[63] F. Herklotz, E. V. Lavrov, and J. Weber, Physica B **407**, 2883 (2012).
[64] K. M. Johansen, A. Zubiaga, F. Tuomisto, E. V. Monakhov, A. Y. Kuznetsov, and B. G. Svensson, Phys. Rev. B **84**, 115203 (2011).
[65] A. M. Hyland, R. A. Makin, S. M. Durbin, and M. W. Allen, J. Appl. Phys. **121**, 024501 (2017).
[66] F. Traeger, M. Kauer, C. Wöll, D. Rogalla, and H.-W. Becker, Phys. Rev. B **84**, 075462 (2011).